Hindawi
Advances in Mathematical Physics
Volume 2023, Article ID 1074719, 11 pages
https://doi.org/10.1155/2023/1074719

Research Article

Computational Fluid Dynamics for Cavity Natural Heat Convection: Numerical Analysis and Optimization in Greenhouse Application

Yin Zhang, Menglong Zhang, Jianwu Xiong, Gang Mao, and Yicong Qi

School of Architecture, Southwest Minzu University, Chengdu 610225, China

Correspondence should be addressed to Yicong Qi; 80300254@swun.edu.cn

Received 29 June 2023; Revised 8 December 2023; Accepted 16 December 2023; Published 29 December 2023

Academic Editor: Onur Alp Ilhan

Natural convection in cavity plays a significant role in energy-related field, including the indoor heat transfer analysis in greenhouse with integrated PV roof. In this study, mathematical model is established for two-dimensional heat transfer analysis in greenhouse air cavity, with numerical simulation through computational fluid dynamics (CFD). Main natural convection impact factors, such as system configuration parameters (tilting angle and PV panel unit number) and fluid thermal–physical properties, are investigated with indoor temperature distribution and streamline comparison by finite-volume method (FVD). Preliminary results show that with rising Rayleigh number (Ra), natural convection is enhanced with growing Nusselt number (Nu). Moreover, panel slope tilting angle (θ) highly determines inside heat transfer subregions in terms of the vertical temperature gradient declines with rising θ, improving the temperature distribution uniformity inside. The solar greenhouse example illustrates that with the increasing numbers of panel group numbers (n), the air temperature gradient differences decrease, improving the temperature distribution uniformity inside, which is preferable to built environment accurate control for greenhouse in the practical engineering. This work can provide modeling method support and reference for natural heat convection applications.

1. Introduction

1.1. Background. Natural convection, known also as free convection is a mechanism, or type of mass and heat transport, in which the fluid motion is generated only by density differences in the fluid occurring due to temperature gradients, not by any external source [1]. In natural convection, fluid surrounding a heat source receives heat and by thermal expansion becomes less dense and rises. Thermal expansion of the fluid plays a crucial role. In other words, heavier components will fall, while lighter components rise, leading to bulk fluid movement [2]. Natural convection can only occur in a gravitational field or in the presence of another proper acceleration.

Similar to the forced convection, also natural convection heat transfer take place both by thermal diffusion (the random motion of fluid molecules) and by advection, in which matter or heat is transported by the larger scale motion of currents in the fluid [3]. At the surface, energy flow occurs purely by conduction, even in convection. It is due to the fact, there is always a thin stagnant fluid film layer on the heat transfer surface. But in the next layers both conduction and diffusion-mass movement in the molecular level or macroscopic level occurs. Due to the mass movement the rate of energy transfer is higher. Higher the rate of mass movement, thinner the stagnant fluid film layer will be and higher will be the heat flow rate [4].

For heat convection analysis, most heat transfer correlations in natural convection are based on the experimental measurements and engineers often use proper characteristic numbers to describe natural convection heat transfer. The characteristic index describing convective heat transfer is the Nusselt number, which is defined as the ratio of heat convection to heat conduction within the fluid [5]. The Nusselt number represents the enhancement of heat transfer through a fluid layer as a result of convection relative to conduction across the same fluid layer. But in the case of free convection, heat transfer correlations are usually expressed in terms of

the Rayleigh number [6]. The Rayleigh number is used to express heat transfer in natural convection. The magnitude of the Rayleigh number is a good indication as to whether the natural convection boundary layer is laminar or turbulent [7]. Therein, air cavity related natural convection configuration can be found in many practical engineering fields, such as solar collector, built environment, industrial or agricultural productions, and various applied energy systems, etc. [8]. There are many literatures focused on the heat transfer dynamic responses in cavity with different boundary conditions, physical property of fluid and configuration parameters of installation [9].

1.2. Literature Review. In many engineering applications, adiabatic or exothermic obstacles which normally were attached to the cavity internal surface, such as exothermic and sedentary human bodies in room, food in refrigerator, fins in heater, etc. The location, shape, and physical properties of these obstacles are complicated, which will affect the structure of fluid flow, and directly change the natural convection heat transfer in the cavity [10]. Ibrahim and Anbessa [11] inspected the mixed convection flow of Eyring–Powell nanofluid over a linearly stretching sheet through a porous medium in the nonlinear differential systems, which are solved using the spectral relaxation method, and then exposed graphically the efficiency of numerous parameters on velocity, temperature, and concentration curves. Sene [12] presented a class of numerical schemes to obtain numerical solutions of the constructive equations of a type of Casson fluid model, with numerical scheme called the fractional version of the Adams Basford numerical procedure. Ikram et al. [13] conducted computational study on the transient conjugate forced convection flow and heat transfer characteristics in a hexagonal, air-filled cavity, equipped with a floor heater of constant heat flux under the rotational influence of an adiabatic flow modulator. Based on that, they expressed the two-dimensional unsteady continuity, momentum, and energy equations in a nondimensional form where the buoyant force was modeled through the Boussinesq approximation through the Arbitrary Lagrangian Euler (ALE) finite element to solve the moving mesh problem by formulating a free triangular discretization scheme [14]. Furthermore, Saboj et al. [15] considered entropy generation within an octagonal cavity subjected to a cold cylinder inside the cavity and solve the dimensionless version of the governing equations and their corresponding boundary conditions numerically using the finite-element method, employing triangular mesh elements for discretization. Saha et al. [16] found that in the domain of a vertical plate, the resulting nonlinear method was mapped and then worked out numerically by applying the implicit central finite difference technique with Newton's quasilinearization method. Hamza et al. [17] examined the effects of magnetohydrodynamics on time-dependent mixed convection flow of an exothermic fluid in a vertical channel and transformed dimensional nonlinear flow equations into dimensionless form with suitable transformation via homotopy perturbation approach.

In addition, various studies natural heat convection has being conducted in both theoretical and application regards, including modified turbulent modeling, computational fluid dynamics (CFD) and simulation, nanomaterial additives for thermal–physical improvement and practical engineering optimization, over recent years [18, 19]. Shanmuganathan et al. [20] experimented on building energy efficiency coupled with reflective coating under natural heat convection boundary conditions. Yu et al. [21] conducted similar simulation on dynamic heat convection performance of a novel ventilated building roof. Sarrafha et al. [22] investigated the transient thermal response of multiwalled phase change materials in building with carbon nanotube for heat transfer enhancement. Saxena et al. [23] studied also underwent experimental assessment on the heat convection effect of phase change material embedded bricks for passive rooms. Zhang et al. [24] then applied expanded graphite/paraffin/silicone rubber to thermal energy storage materials and revealed the heat convection impact mechanism behind the fluid thermal properties. Umair et al. [25] proposed stable phase change composites supported by a biomass-derived carbon scaffold with multiple energy conversion abilities and emphasized on the system configuration parameters influence. Furthermore, Sheng et al. [26] conducted CFD on the natural convections with honeycomb carbon fibers strengthened composite phase change materials for the superior thermal energy storage.

In practical engineering fields, natural heat convection modeling and experimental studies in industrial, agricultural sectors have drawn increasing attentions during recent years, toward sustainable production and development transition [27–29]. For instance, solar greenhouses incorporate special design features to maximize use of the sun's heat so they can run without an input of energy, which makes it a potential research and application hotspots for renewable and eco-friendly farm construction [30]. The solar room design needs to do two things in order to achieve a comfortable growing temperature year-round: first, to maximize the use of the sun's heat and light and second, to create "thermal mass" effect elements that do not change temperature easily, to stabilize the indoor temperature with inside heat convection considerations [31]. Ghosh [32] summarized the main features and deign approaches for both passive and active solar rooms in various building sectors and found that even solar PV applications were favorable for the electricity generation to reduce domestic consumption, the indoor thermal response also highly depended on the heat convection among PV panels, building envelopes, and indoor air. Taşer et al. [33] simulated the indoor temperature of the greenhouse based on the unsteady heat transfer theory and optimized the geometrical factors and the envelope structure, contributing to the improvement of the structure and the temperature environment of the solar greenhouse and the reduction of capital cost. As the most efficient energy conserving greenhouse, the single slope solar greenhouse which always orients south or south by east or west within 15° and has a transmissive south roof has become the typical Chinese greenhouse and gained its popularity in middle and north China [34]. By making full use of the solar energy and preserving heat closely with good thermal insulation, it can keep the indoor temperature of 25–30°C higher than the ambient temperature and can produce

vegetables in winter with no or little supplementary energy, achieving high-economic benefit with no or little pollution [35].

1.3. Research Focus. As reported, even though there are abundant available research on natural heat convection analysis from theoretical, modeling, simulation, and experiment perspectives. For specific engineering application occasion, such as indoor environment control in solar greenhouse, the detailed dynamic thermal response in the cavity air under PV roof heat convection consideration still need further investigation, since the indoor temperature distribution is significantly influenced by the design parameters for certain solar greenhouses.

In this paper, the mathematical model is established for two-dimensional heat transfer analysis in greenhouse cavity, with numerical simulation via CFD. Main natural convection impact factors, such as system configuration parameters (tilting angle and PV panel unit number) and fluid thermal–physical properties, are investigated with indoor temperature distribution and streamline comparison by finite-volume simulation solution method. This work can provide theoretical support and reference for natural heat convection applications in the engineering field.

2. Methodology

2.1. Physical Description. Due to the temperature difference within the fluid caused by the density difference and the formation of buoyancy force, in this buoyancy force triggered by the movement of the heat transfer process, also known as free motion heat transfer, and the surrounding air is natural convection heat transfer. Its strength depends on the fluid flow along the solid heat transfer surface state and its development, and these and the fluid flow space and heat transfer surface shape, size, surface, and temperature difference between the fluid, the type of fluid and physical parameters and many other factors, is a complex process affected by many factors. Figure 1 shows the schematic diagram of a typical greenhouse on solar farms for agriculture or domestic production. The integrated photovoltaic panels are installed on the roof slope with certain tilting angle for solar energy collection and conversion during daytime, which could make the surface temperature of the PV roof become much higher than that of indoor air. Hence, the natural heat convection in the air cavity significantly impacts the indoor thermal environment. The PV roof surfaces are maintained at high temperature T_h, the boundaries of cavity surface are maintained at relatively low temperature T_c ($T_h > T_c$). The tilting angle of PV roof slope is designated as θ. The system is considered incompressible (constant property fluid), steady-state, Newtonian and the Boussinesq approximation is applied for fluid with constant physical properties. It is assumed that the plates array is assumed to exchange heat by convection with surrounding fluid, and the radiation effect can be taken to be negligible. The gravitational acceleration acts in the negative y-direction.

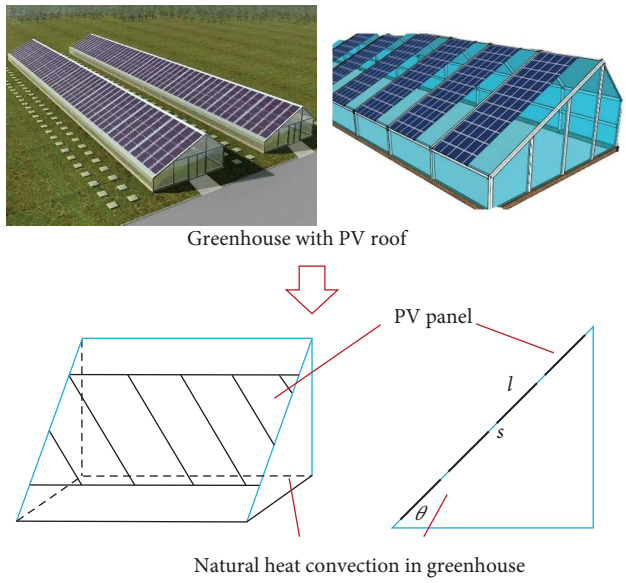

FIGURE 1: Schematic diagram of cavity computational model for natural heat convection in greenhouse.

2.2. Mathematical Model. The process of homogenizing the temperature of a liquid or gas by circulating between the hotter and cooler parts of the liquid or gas. Convection is a unique way of heat transfer in liquids and gases, and the convection phenomenon of gases is more obvious than that of liquids. Convection can be divided into natural convection and forced convection. Natural convection tends to occur naturally and is caused by temperature inhomogeneity. Forced convection is formed due to external influences on the fluid agitation. Increasing the flow rate of a liquid or gas can accelerate convective heat transfer. Natural convection is also divided into laminar and turbulent flow. In the case of laminar flow, the thermal resistance of heat transfer depends entirely on the thickness of the thin layer. Starting from the lower end of the heat transfer wall, the thickness of the laminar thin layer increases with increasing height. In contrast, the local surface heat transfer coefficient decreases with increasing height. If the wall is high enough, the fluid flow will gradually change into the turbulent flow. The heat transfer law changes during turbulent flow. It has been shown that the local surface heat transfer coefficient during vigorous turbulence is almost a constant. According to the classical heat transfer theory and basic principles [36–38], dimensionless governing equations can be obtained via introducing dimensionless variables as follows:

$$X = \frac{x}{l},\ Y = \frac{y}{l},\ \Theta = \frac{T - T_c}{T_h - T_c},\ U, V = \frac{(u, v)l}{\alpha},\ u = -\frac{\partial \psi}{\partial y},$$
$$v = \frac{\partial \psi}{\partial x},\ P = \frac{pl^2}{\rho \alpha^2},\ Ra = \frac{\beta g (T_h - T_c) l^3 Pr}{\nu^2},\ Pr = \frac{\nu}{\alpha}. \quad (1)$$

The governing equations for the problem under consideration are based on the balance laws of mass, linear momentum, and energy in two dimensions and steady state [36–38]. Following the previous assumptions, these equations can be written in dimensionless form as follows:

$$\frac{\partial U}{\partial X}+\frac{\partial V}{\partial Y}=0, \tag{2}$$

$$U\frac{\partial U}{\partial X}+V\frac{\partial U}{\partial Y}=-\frac{\partial P}{\partial X}+Pr\left(\frac{\partial^2 U}{\partial X^2}+\frac{\partial^2 U}{\partial Y^2}\right), \tag{3}$$

$$U\frac{\partial V}{\partial X}+V\frac{\partial V}{\partial Y}=-\frac{\partial P}{\partial Y}+Pr\left(\frac{\partial^2 V}{\partial X^2}+\frac{\partial^2 V}{\partial Y^2}\right)+Ra\cdot Pr\cdot \Theta, \tag{4}$$

$$U\frac{\partial \Theta}{\partial X}+V\frac{\partial \Theta}{\partial Y}=\frac{\partial^2 \Theta}{\partial X^2}+\frac{\partial^2 \Theta}{\partial Y^2}. \tag{5}$$

The dimensionless form of boundary conditions for the calculation domain are as follows.

For the bottom surface (cold):

$$U=0, V=0, \partial\theta/\partial n=0. \tag{6}$$

For the PV roof (hot):

$$U=V=0, \theta=1. \tag{7}$$

For the rest cavity space:

$$U=V=0, \theta=0. \tag{8}$$

Nusselt number is regarded as the evaluation index for heat transfer intensity [36–38]. The local Nusselt number can be expressed by:

$$Nux=-\delta n\left(\frac{\partial \delta}{\partial \mathrm{X}}U_x+\frac{\partial \theta}{\partial Y}V_y\right). \tag{9}$$

Mean Nusselt number is as follows:

$$Nu=\frac{1}{l}\int_0^l Nux. \tag{10}$$

2.3. Numerical Method and Validation. The governing equations were solved using the finite-volume method (FVM). It is assumed a particularly prominent role in the simulation of fluid flow problems and related transport phenomena. FVM work done by the computer fluid dynamic group at Imperial College in the early 70 s under the direction of Professor Spalding, with contributors as Patanka, which then has been widely used for the CFD [36]. This technique is based on the discretization of the governing equations using the central difference in space. The discretization equations were solved by the Gauss–Seidel model with super relaxation factor. The iteration method used in this program is a line-by-line procedure, which is a combination of the direct method and the resulting tridiagonal matrix algorithm (TDMA), which is more suitable for fluid computation than the finite-difference method and the finite-element method, and is able to overcome the disadvantage of the discrete Taylor expansion with good conservatism, as well as adapting well to the mesh and more easily obtaining smooth results [15–17]. Moreover, the point where the heater meets the rest of the section, i.e., the hot/cold junction, can become a singularity in the numerical calculations, and the FVM solves this problem by taking the mean value of the temperature at this point (Figure 2).

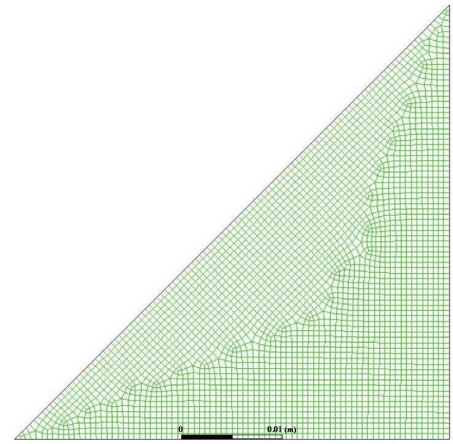

Figure 2: Mesh grid for computational fluid dynamics in cavity.

Commercial software Fluent 22 is used to proceed numerical solution in this paper. The aforementioned system of equations with matching boundary and initial conditions are discretized by the FVD. The SIMPLE algorithm is applied to cope with the pressure–velocity coupling. Least squares cell based and body force weight schemes are, respectively, utilized in gradient and pressure interpolation, which are applicable to strongly swirling flows. Second order upwind scheme is employed to discretize the diffusion and convective terms in momentum and energy equations. Second-order implicit transient formulation is selected and all the under-relaxation factors remain at default values. The derived algebraic systems of equations after discretization are solved based on TDMA iteratively until the absolute residuals are less than the convergence requirement. In order to check the accuracy of the numerical results obtained in this problem, a numerical experiment performed by Koca et al. [37, 38] was chosen as the target of this simulation–validation comparison for the reason that the comparison object should be relevant to the physical model of this paper: the local Nussle number of a right-angled triangular cavity with $Ra=1.5^{*}\times 10^{4}$. The number of mesh edges per unit length is defined as the mesh density k. Figure 3 illustrates the simulation results for the three different mesh densities as well as the literature data. It can be clearly seen that the results at $k=1$ are not smooth enough and have a large degree of deviation, the results at $k=2$ and $k=4$ have a high degree of overlap, and considering the

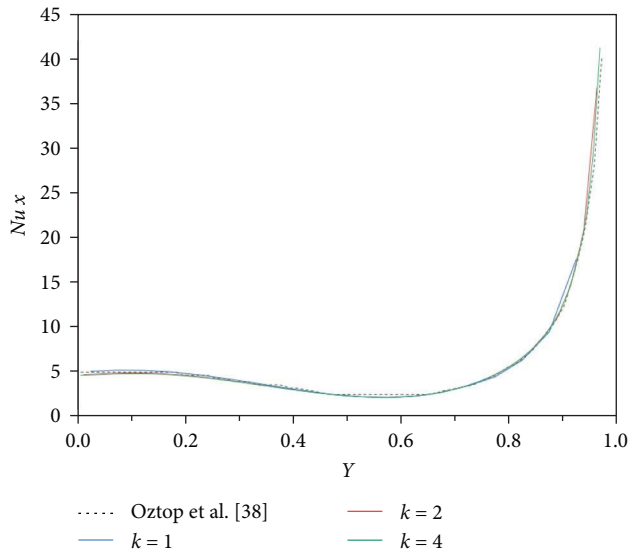

Figure 3: Independent test of grid number and model validation [37, 38].

Table 1: CFD grid test of different cells number ($Ra = 10^6$, $\theta = 45°$).

Cell numbers	Nu	$\lvert\Psi\rvert_{max}$	ΔNu	$\Delta\lvert\Psi\rvert_{max}$
1,610	7.213	63.120	6.86%	4.50%
4,320	7.708	65.953	1.26%	0.05%
14,610	7.805	66.437	0.00%	0.01%
19,825	7.806	66.912	—	—

computational efficiency, the mesh at $k = 2$ has been able to achieve a satisfactory accuracy. In addition, the simulation results are in good agreement with the literature data. Moreover, in order to investigate the Ra impact on heat convection effect, the mesh grid test is also performed under the considered maximal $Ra = 10^6$ here. As Table 1 listed, the average Nu number of cells of 14,610 and 19,825 gives nearly identical results ($Ra = 10^6$, $\theta = 45°$). Considering both the accuracy and the computational time, 14,610 nodes were used in this paper.

3. Results and Discussion

3.1. Heat Transfer Influence Factors. According to the previous proposed heat-transfer model, the influence mechanisms of installation parameters for the PV panels arrays can be investigated, including array group numbers and roof-tilting angle. As Figure 4 shows, typical case scenarios are designated for comparative study, with different PV array numbers and dimensionless size on the roof slope.

Figures 5 and 6 gives the simulation results of the temperature distribution and streamline compiles in the air cavity with high-temperature PV roof panels, respectively. According to Equation (1), the dimensionless temperatures vary widely inside, indicating high nonuniformity due to the natural heat convection effect. The vicinity air around PV plates area approaches to isothermal with the maximal temperature, about two times higher than that near the vertical cold side.

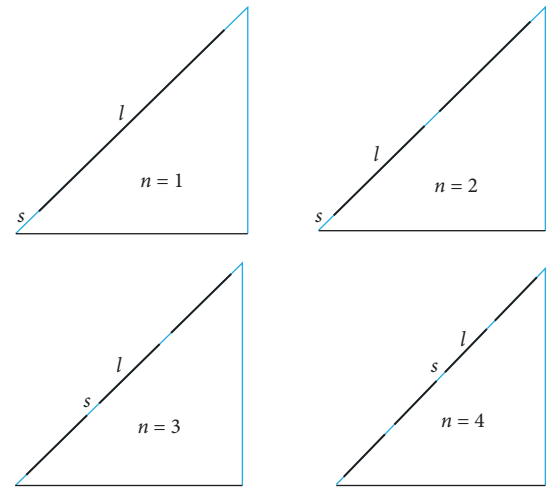

Dimensionless size

	l	s
$n = 1$	4/5	1/10
$n = 2$	2/5	1/15
$n = 3$	4/15	1/20
$n = 4$	1/5	1/25

Figure 4: Case scenarios for natural convection comparison.

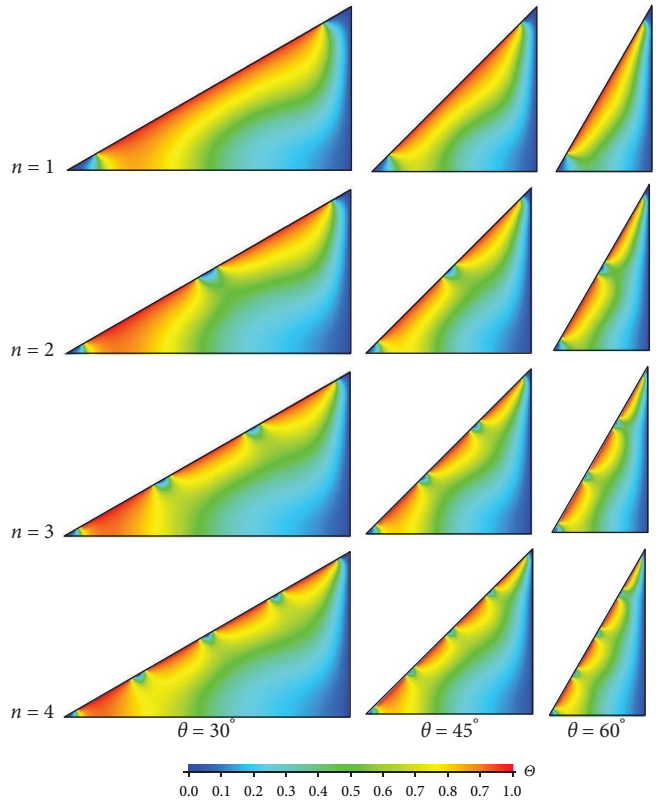

Figure 5: Dimensionless temperature distribution under natural heat convection ($Ra = 10^4$).

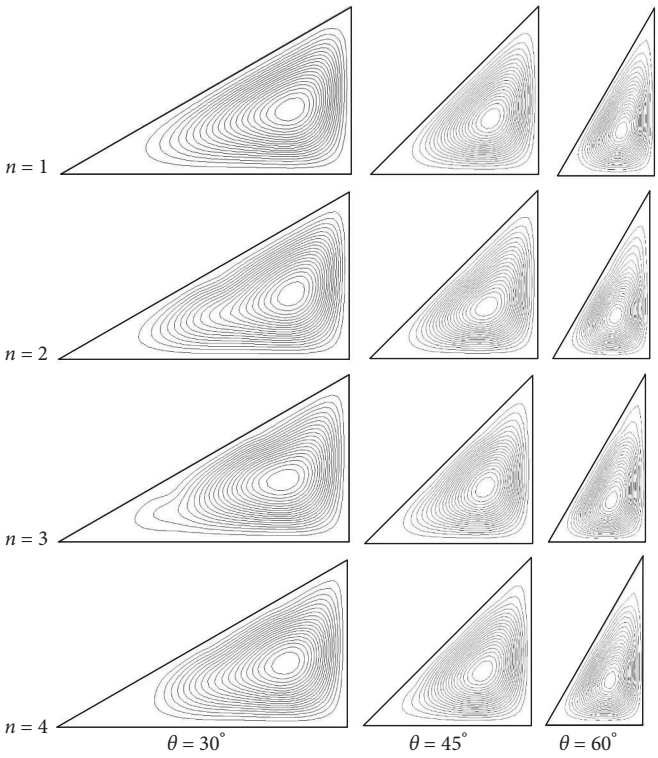

Figure 6: Streamlines compile under natural heat convection ($Ra = 10^4$).

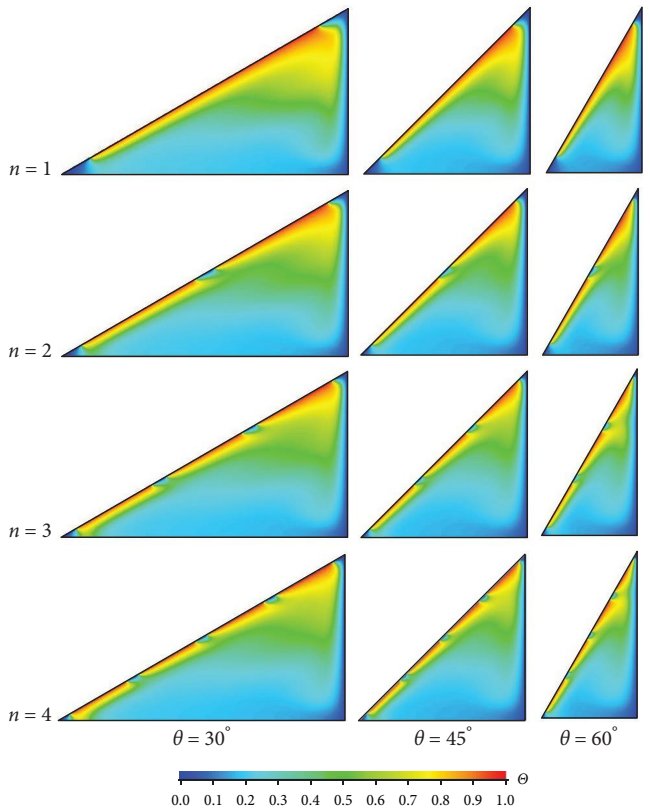

Figure 7: Dimensionless temperature distribution under natural heat convection ($Ra = 10^6$).

Due to the temperature difference between the various parts of the triangular cavity wall surface, there is a natural convection in the cavity at this time, the isotherm especially at the bottom to the oblique edge of the curved, indicating that the air flows upward when it is near the oblique edge, and downward when it is close to the vertical edge. However, the natural convection in the cavity is relatively weak, and heat conduction is dominant, therefore, the isotherm is smooth and the distribution is relatively uniform. There is a flow cell in the cavity, and the core of the vortex is elliptical and located in the center of the cavity. The streamlines are uniformly distributed and there is essentially no flow at the bottom and top corners, further indicating that the natural convection is of little strength.

According to fluid mechanics basic principles, the Rayleigh number (Ra) of a fluid is a dimensionless number associated with buoyancy-driven convection (also known as free or natural convection). When the Rayleigh number of a fluid is below a critical value, the main form of the heat transfer is heat conduction, whereas when the Rayleigh number exceeds the critical value the main form of the heat transfer is convection. Therefore, Figures 7 and 8 gives the temperature distribution and streamline compiles in the air cavity when Ra number rises from 10^4 to 10^6 as comparison. It is clear that the natural convection inside the cavity is significantly enhanced with rising Ra number. The isotherms near the oblique edge have an upward tendency, while the isotherms near the vertical edge have a downward tendency prism, as the main region of the whole temperature cloud map changes from left–right stratification to up–down

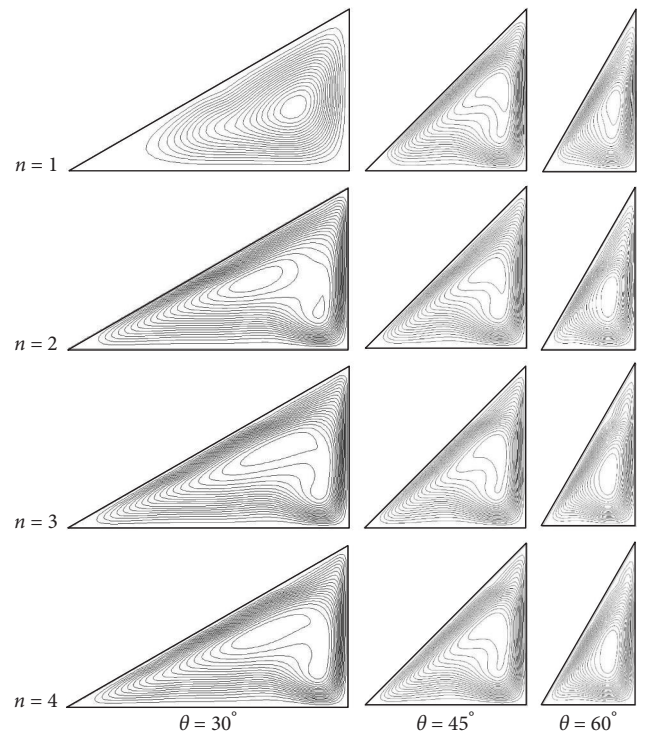

Figure 8: Streamlines compile under natural heat convection ($Ra = 10^6$).

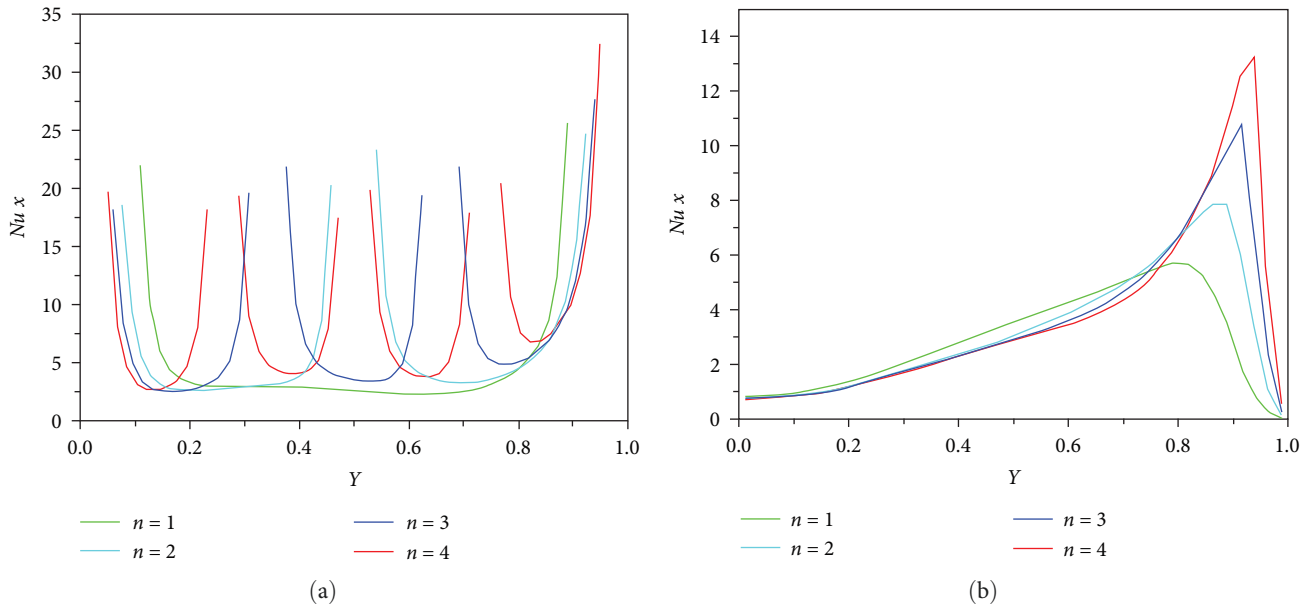

FIGURE 9: Local *Nu* variations with changing panel unit numbers and slope tilt angles ($Ra = 10^4$, $\theta = 45°$): (a) hot surface and (b) cold surface.

stratification, compared with the case of $Ra = 10^4$ (Figures 5 and 6). For the same reason, when each solar panel is viewed individually, the temperature layer in the higher temperature range shows a regular gradual thickening from bottom to top.

3.2. Nu Number Comparison. There are two heat transfer effects in the whole triangular cavity and interact with each other: one is the heat transfer between the hot and cold surfaces on the slanted side, and the other is the heat transfer between the hot surface and the vertical side edges. Figure 9 gives the *Nu* variations with changing panel unit numbers and slope tilt angles ($Ra = 10^4$). The dense presence of isotherms near the contact site of the hot and cold wall surfaces of the sloping edge, with larger temperature gradients and stronger heat transfer, can be observed as a larger local Nussle number near the contact site; $n = 1$. The local Nussle number in the middle region of the heater remains essentially constant due to natural convection, and the increase in the number of isotherms leads to more frequent changes in the temperature gradient along the hot edge, which eliminates this stability. In addition, as the dimensionless value Y increases, the heat transfer between the heater and the vertical edge is enhanced, and under the combined effect, the local Nussell number curve shows an upward trend along Y in the whole. An increase in the number of equal fractions implies an increase in the number of contacts between the hot and cold wall surfaces of the sloping edge, and an increase in the area of its adjoining region where a high-density temperature gradient exists, leading to an increase in the overall heat transfer intensity.

On the other hand, as the PV panel unit number n increases, the average Nussle number of hot surface shows a nearly linear increase, which also leads to an increase in the average Nussle number of vertical edges (cold surface) with

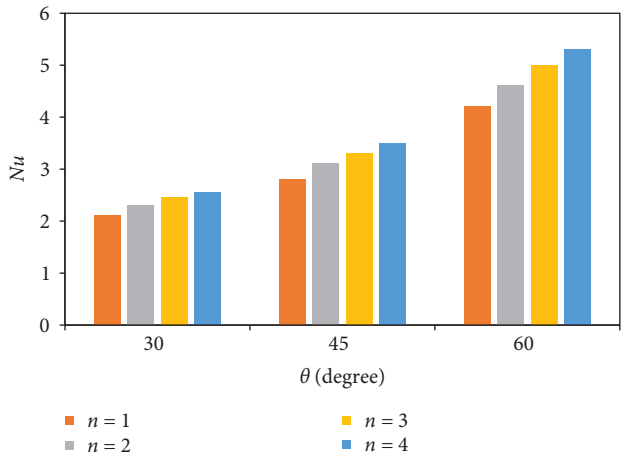

FIGURE 10: Average *Nu* variations with changing panel numbers and slope tilt angles ($Ra = 10^4$).

relatively lower growth rate. Moreover, Figure 9(b) indicates that the local Nussle number under different isotherms increases first slightly and then decreases after reaching the peak value. It is because the heat transfer phenomenon between the hot and cold wall surfaces of the slanting side induces a high-temperature region of the hot side to be compressed, the isotherms are slightly shifted to the left in general, and the temperature gradient of the lower region of the vertical side decreases slightly, and the change of local Nusslet number is more drastic in the top region of the triangular cavity, the upper heater is gradually shifted to the top with the increase of isotherms in layout.

Figure 10 gives the average *Nu* value variation trends inside cavity regions. For one thing, the tilt angle greatly impacts the temperature gradient formation in the cavity,

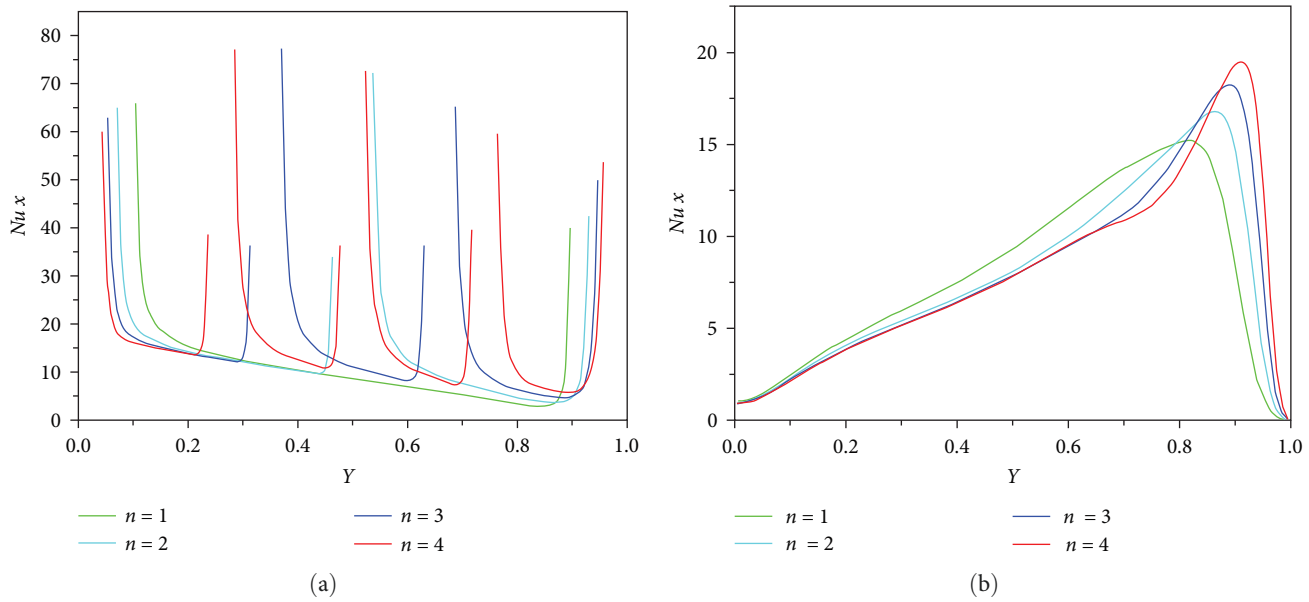

Figure 11: Local *Nu* variations with changing panel unit numbers and slope tilt angles ($Ra = 10^6$, $\theta = 45°$): (a) hot surface and (b) cold surface.

which in turn affects the heat transfer process and the degree of interaction between the various parts of the heat transfer. With decreasing tilt angle, the *Nu* increases at the two ends whereas decreases in the middle, on the PV panel slope. The temperature variation trend in the top region of the triangular cavity is more sensitive to tilt angle change due to the air heat buoyancy effect inside. For another, with the growing numbers of array group numbers, the temperature gradient declines in the cavity, improving the temperature distribution uniformity inside, which is preferable to built environment accurate control for greenhouse in the practical engineering.

3.3. Ra Number Comparison. According to the aforementioned analysis, both system configurations (panel unit number, tilting angle) and indoor air thermal–physical properties (*Ra*) significantly impact the cavity heat transfer inside. To investigate the heat-convection effect and mechanism from fluid mechanics perspective, it is assumed no solar panels on the slope for heating in the sebsection. Figure 11 gives the *Nu* variations with changing panel unit numbers and slope tilt angles ($Ra = 10^6$). Compared to Figure 9, the local *Nu* curves show similar changing trends for both the hot and cold surfaces when *Ra* growing from 10^4 to 10^6. In the top region of the triangular cavity, the local Nusslet number changes more drastically, the upper heater is gradually shifted to the top with the increase in the number of isotherms in the layout, and the influence of the heater position on the heat transfer intensity cannot be ignored because the distance between the heater and the vertical edge is small enough, and the maximum value of the local Nussle number varies greatly, while the position of the maximum value shifts in the direction of the *Y* value increasing. The increase in the number of equal fractions has less effect on the flow line, and the overall distribution remains basically unchanged, except that the flow line near the slanting edge is slightly pitted, which is due to the alternation of hot and cold surfaces on the slanting edge that leads to an uneven temperature difference between the neighboring area and the area near the vertical edge, and the buoyancy driven by the temperature difference is uneven, which leads to an uneven flow rate.

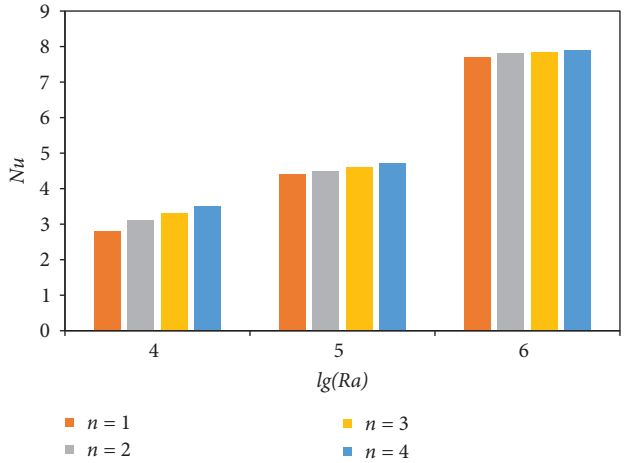

Figure 12: Average *Nu* variations with changing panel numbers and *Ra* numbers ($\theta = 45°$).

On the other hand, Figure 12 gives the average *Nu* variation trends inside cavity regions with changing *Ra* numbers. It is clear that for the same system configurations (PV panel group number *n* and tilting angle θ), the cavity air average *Nu* significantly rises with growing *Ra*, due to the strengthened natural heat convection inside. Moreover, the *Nu* becomes less sensitive to *n* when *Ra* increases from 10^4 to 10^6. It indicates that for cavity air dominant by heat convection, *Ra* is the key influence factor on inside heat transfer intensity and temperature distribution.

4. Conclusions

In this paper, heat-transfer model is built for two-dimensional natural convection in greenhouse cavity with CFD analysis. Main heat convection impact factors, including system configuration parameters (tilting angle and PV panel unit number) and fluid thermal–physical properties, are investigated with indoor temperature distribution and streamline comparison through FVM. According to the numerical and comparative analysis, key conclusions can be drawn in to the following short bullets:

(1) For heat transfer intensity, Nusselt number (Nu) always increases with rising Rayleigh number (Ra). Generally speaking, as the Rayleigh number increases, the natural convection is enhanced with denser streamlines, and the heat transfer in the air cavity turns to be mainly dominant by the heat convection.

(2) Panel slope tilting angle (θ) highly determines inside subregions with different natural convection intensity. The temperature variation trend in the top region of the triangular cavity is more sensitive to the tilting angle change due to the air heat buoyancy effect inside. With the growing θ, the vertical temperature gradient declines, improving the temperature distribution uniformity inside.

(3) For the solar greenhouse application, with the growing numbers of panel group numbers (n), the air temperature gradient differences decline, improving the temperature distribution uniformity inside, which is preferable to built environment accurate control for greenhouse in the practical engineering.

The present study focuses on certain case to illustrate the natural heat convection in air cavity in solar greenhouse applications. The current limitations of the case-based analysis also arise further studies in the next research stages: (1) influence of Re, Gr, and Pr on natural heat convection; (2) combined heat transfer process involving conductivity, enforced convection and thermal radiation; and (3) other engineering application situations.

Nomenclature

Symbols

g: Gravitational acceleration (m/s^2)
n: Group number of PV panels
l: Length (m)
L: Nondimensional length
Nu: Nusselt number
p: Pressure (Pa)
P: Nondimensional pressure
Pr: Prandtl number
Ra: Rayleigh number
T: Temperature (K)
u, v: Velocity (m/s)
U, V: Nondimensional velocity

Subscript

c: Cold
h: Hot

Greek Symbols

α: Thermal diffusivity (m^2/s)
β: Thermal expansion coefficient (1/K)
Θ: Nondimensional temperature
ψ: Nondimensional streamline function
θ: Slope tilting angle (°).

Data Availability

Data supporting this research article are available on request.

Disclosure

The funders had no role in the design of the study; in the collection, analyses, or interpretation of data; in the writing of the manuscript; or in the decision to publish the results.

Conflicts of Interest

The authors declare that they have no conflicts of interest.

Acknowledgments

This work is supported by the National Natural Science Foundation of China (no. 52308038) and the Higher Education Reform Research Project of National Ethnic and Religious Affairs Commission of China (no. 23022).

References

[1] D. Nie, "Quasilinear hyperbolic systems applied to describe the magnetohydrodynamic nanofluid flow," *Advances in Mathematical Physics*, vol. 2023, Article ID 4349646, 10 pages, 2023.

[2] A. Ranjha and G. Kaddoum, "URLLC facilitated by mobile UAV relay and RIS: a joint design of passive beamforming, blocklength, and UAV positioning," *IEEE Internet of Things Journal*, vol. 8, no. 6, pp. 4618–4627, 2020.

[3] M. Samir, S. Sharafeddine, C. M. Assi, T. M. Nguyen, and A. Ghrayeb, "UAV trajectory planning for data collection from time-constrained IoT devices," *IEEE Transactions on Wireless Communications*, vol. 19, no. 1, pp. 34–46, 2020.

[4] T. Saha, G. Saha, N. Parveen, and T. Islam, "Unsteady magneto-hydrodynamic behavior of TiO2-kerosene nanofluid flow in wavy octagonal cavity," *International Journal of Thermofluids*, vol. 21, Article ID 100530, 2024.

[5] M. Cimmino, "An approximation of the finite line source solution to model thermal interactions between geothermal boreholes," *International Communications in Heat and Mass Transfer*, vol. 127, Article ID 105496, 2021.

[6] C. Prieto and M. Cimmino, "Thermal interactions in large irregular fields of geothermal boreholes: the method of

equivalent boreholes," *Journal of Building Performance Simulation*, vol. 14, no. 4, pp. 446–460, 2021.

[7] A. Rosato, A. Ciervo, G. Ciampi, M. Scorpio, F. Guarino, and S. Sibilio, "Impact of solar field design and back-up technology on dynamic performance of a solar hybrid heating network integrated with a seasonal borehole thermal energy storage serving a small-scale residential district including plug-in electric vehicles," *Renewable Energy*, vol. 154, pp. 684–703, 2020.

[8] H. Mahon, D. O'Connor, D. Friedrich, and B. Hughes, "A review of thermal energy storage technologies for seasonal loops," *Energy*, vol. 239, Article ID 122207, 2022.

[9] A. Dahash, F. Ochs, M. B. Janetti, and W. Streicher, "Advances in seasonal thermal energy storage for solar district heating applications: a critical review on large-scale hot-water tank and pit thermal energy storage systems," *Applied Energy*, vol. 239, pp. 296–315, 2019.

[10] G. Saha, A. A. Y. Al-Waaly, M. C. Paul, and S. C. Saha, "Heat transfer in cavities: configurative systematic review," *Energies*, vol. 16, no. 5, Article ID 2338, 2023.

[11] W. Ibrahim and T. Anbessa, "Hall and ion slip effects on mixed convection flow of Eyring-Powell nanofluid over a stretching surface," *Advances in Mathematical Physics*, vol. 2020, Article ID 4354860, 16 pages, 2020.

[12] N. Sene, "A numerical algorithm applied to free convection flows of the casson fluid along with heat and mass transfer described by the caputo derivative," *Advances in Mathematical Physics*, vol. 2021, Article ID 5225019, 11 pages, 2021.

[13] M. M. Ikram, G. Saha, and S. C. Saha, "Conjugate forced convection transient flow and heat transfer analysis in a hexagonal, partitioned, air filled cavity with dynamic modulator," *International Journal of Heat and Mass Transfer*, vol. 167, Article ID 120786, 2021.

[14] M. M. Ikram, G. Saha, and S. C. Saha, "Unsteady conjugate heat transfer characteristics in hexagonal cavity equipped with a multi-blade dynamic modulator," *International Journal of Heat and Mass Transfer*, vol. 200, Article ID 123527, 2023.

[15] J. H. Saboj, P. Nag, G. Saha, and S. C. Saha, "Entropy production analysis in an octagonal cavity with an inner cold cylinder: a thermodynamic aspect," *Energies*, vol. 16, no. 14, Article ID 5487, 2023.

[16] T. Saha, N. Parveen, and T. Islam, "Analysis of reciprocal thermal conductivity on free convection flow along a wavy vertical surface," *Advances in Mathematical Physics*, vol. 2022, Article ID 6389275, 12 pages, 2022.

[17] M. M. Hamza, S. Abdulsalam, and S. K. Ahmad, "Time-dependent magnetohydrodynamic (MHD) flow of an exothermic arrhenius fluid in a vertical channel with convective boundary condition," *Advances in Mathematical Physics*, vol. 2023, Article ID 7173925, 13 pages, 2023.

[18] T. Saha, T. Islam, S. Yeasmin, and N. Parveen, "Thermal influence of heated fin on MHD natural convection flow of nanofluids inside a wavy square cavity," *International Journal of Thermofluids*, vol. 18, Article ID 100338, 2023.

[19] H. G. Kim, Y.-S. Kim, L. K. Kwac, M. Park, and H. K. Shin, "Role of phase change materials containing carbonized rice husks on the roof-surface and indoor temperatures for cool roof system application," *Molecules*, vol. 25, no. 14, Article ID 3280, 2020.

[20] R. Shanmuganathan, M. Sekar, T. R. Praveenkumar, A. Pugazhendhi, and K. Brindhadevi, "Experimental investigation and numerical analysis of energy efficiency building using phase changing material coupled with reflective coating," *International Journal of Energy Research*, vol. 45, no. 12, pp. 17279–17290, 2021.

[21] J. Yu, K. Leng, F. Wang, H. Ye, and Y. Luo, "Simulation study on dynamic thermal performance of a new ventilated roof with form-stable PCM in Southern China," *Sustainability*, vol. 12, no. 22, Article ID 9315, 2020.

[22] H. Sarrafha, A. Kasaeian, M. H. Jahangir, and R. A. Taylor, "Transient thermal response of multi-walled carbon nanotube phase change materials in building walls," *Energy*, vol. 224, Article ID 120120, 2021.

[23] R. Saxena, D. Rakshit, and S. C. Kaushik, "Experimental assessment of phase change material (PCM) embedded bricks for passive conditioning in buildings," *Renewable Energy*, vol. 149, pp. 587–599, 2020.

[24] Y. Zhang, W. Li, J. Huang, M. Cao, and G. Du, "Expanded graphite/paraffin/silicone rubber as high temperature form-stabilized phase change materials for thermal energy storage and thermal interface materials," *Materials*, vol. 13, no. 4, Article ID 894, 2020.

[25] M. M. Umair, Y. Zhang, A. Tehrim, S. Zhang, and B. Tang, "Form-stable phase-change composites supported by a biomass-derived carbon scaffold with multiple energy conversion abilities," *Industrial & Engineering Chemistry Research*, vol. 59, no. 4, pp. 1393–1401, 2020.

[26] N. Sheng, Z. Rao, C. Zhu, and H. Habazaki, "Honeycomb carbon fibers strengthened composite phase change materials for superior thermal energy storage," *Applied Thermal Engineering*, vol. 164, Article ID 114493, 2020.

[27] P. Agarwal and A. Prabhakar, "Energy and thermo-economic analysis of PCM integrated brick in composite climatic condition of Jaipur—a numerical study," *Sustainable Cities and Society*, vol. 88, Article ID 104294, 2023.

[28] M. K. Gupta, P. K. S. Rathore, R. Kumar, and N. K. Gupta, "Experimental analysis of clay bricks incorporated with phase change material for enhanced thermal energy storage in buildings," *Journal of Energy Storage*, vol. 64, Article ID 107248, 2023.

[29] S. Fathi and A. Kavoosi, "Effect of electrochromic windows on energy consumption of high-rise office buildings in different climate regions of Iran," *Solar Energy*, vol. 223, pp. 132–149, 2021.

[30] S. Sarihi, F. M. Saradj, and M. Faizi, "A critical review of façade retrofit measures for minimizing heating and cooling demand in existing buildings," *Sustainable Cities and Society*, vol. 64, Article ID 102525, 2021.

[31] S. Preet, J. Mathur, and S. Mathur, "Influence of geometric design parameters of double skin façade on its thermal and fluid dynamics behavior: a comprehensive review," *Solar Energy*, vol. 236, pp. 249–279, 2022.

[32] A. Ghosh, "Potential of building integrated and attached/applied photovoltaic (BIPV/BAPV) for adaptive less energy-hungry building's skin: a comprehensive review," *Journal of Cleaner Production*, vol. 276, Article ID 123343, 2020.

[33] A. Taşer, B. K. Koyunbaba, and T. Kazanasmaz, "Thermal, daylight, and energy potential of building-integrated photovoltaic (BIPV) systems: a comprehensive review of effects and developments," *Solar Energy*, vol. 251, pp. 171–196, 2023.

[34] A. Khatibi, M. H. Jahangir, and F. R. Astaraei, "Energy and comfort evaluation of a novel hybrid control algorithm for smart electrochromic windows: a simulation study," *Solar Energy*, vol. 241, pp. 671–685, 2022.

[35] Z. Ding, W. Wu, and M. Leung, "Advanced/hybrid thermal energy storage technology: material, cycle, system and perspective," *Renewable and Sustainable Energy Reviews*, vol. 145, Article ID 111088, 2021.
[36] A. Majumdar, *Handbook of Heat Transfer*, McGraw-Hill, New York, NY, USA, 1998.
[37] A. Koca, H. F. Oztop, and Y. Varol, "The effects of Prandtl number on natural convection in triangular enclosures with localized heating from below," *International Communications in Heat and Mass Transfer*, vol. 34, no. 4, pp. 511–519, 2007.
[38] H. F. Oztop, Y. Varol, A. Koca, and M. Firat, "Experimental and numerical analysis of buoyancy-induced flow in inclined triangular enclosures," *International Communications in Heat and Mass Transfer*, vol. 39, no. 8, pp. 1237–1244, 2012.